Modeling Transdermal Permeation. Part I. Predicting Skin Permeability of Both Hydrophobic and Hydrophilic Solutes

Longjian Chen
College of Engineering, China Agricultural University, Beijing 100083, P. R. China

Guoping Lian
Unilever R&D, Colworth, Sharnbrook, Bedford MK44 1LQ, U.K

Lujia Han
College of Engineering, China Agricultural University, Beijing 100083, P. R. China

DOI 10.1002/aic.12048
Published online October 13, 2009 in Wiley InterScience (www.interscience.wiley.com).

In this study, we present a modeling study on the prediction of transdermal permeability of both hydrophobic and hydrophilic solutes, using our recently reported mechanistic model of mass transfer in complex media, where the heterogeneous structure of the stratum corneum is represented by "bricks-and-mortar" model. The partition and diffusion properties of solutes in lipid matrix and corneocytes are calculated separately, without fitting to the modeled skin permeability data. Skin permeability has been predicted for a comprehensive experimental data set of chemicals compiled earlier. When the transcellular pathway is included, the agreement between predicted skin permeability and experimental data is much improved. The improvement is mainly due to better predicted results for hydrophilic solutes. The contribution of each pathway to the overall skin permeability has also been analyzed. The results showed that the transcellular pathway is important not only for highly hydrophilic solutes, but also for moderately hydrophobic solutes. © 2009 American Institute of Chemical Engineers *AIChE J,* 56: 1136–1146, 2010

Keywords: computer model, partition, permeability, stratum corneum, transdermal delivery

Introduction

Human skin is an important organ. The main function of human skin is to keep water in and external substances out of the body. The barrier property of human skin is important to a number of applications including transdermal delivery of drugs, formulation design of skincare products, and risk assessment of hazardous chemical-exposure. There has been an increasing interest in understanding the barrier properties of human skin and a great number of experimental studies have been reported involving both in vivo and in vitro methods.[1–5] Of particular interest on the subject is, the modeling and prediction of transdermal permeation and absorption. This is partly due to ethical difficulties with respect to human and animal experiments and partly due to economic considerations and increasing legislation in the risk assessment of industrial chemicals. A number of mathematical models have been proposed to predict skin permeability of

Correspondence concerning this article should be addressed to L. Han at clj1020@googlemail.com

solutes.[2,6–12] Several reviews on various mathematical models have been reported.[13–15] Most models are quantitative structure and permeability relationship (QSPR) models which correlate skin permeability to physicochemical properties and molecular structures by fitting to experimentally measured data. Early QSPR models correlate skin permeability (K_p) to the lipophilic property of solutes (octanol–water partition coefficient, K_{ow}, and molecular weight, M_W).[11,15,16] Later models have used molecular structure descriptors and functional group contributions.[6,7,12,17] We[18] recently evaluated several frequently quoted QSPR models using a comprehensive data set compiled from the literature and found that the early simple QSPR model of Puts & Guy[11] gives better prediction than the later proposed more complex QSPR models. It is also noticed that QSPR models generally under-predict the skin permeability of hydrophilic solutes by several orders of magnitudes. Although transdermal delivery of hydrophilic solutes is generally slow, under-prediction of their skin permeability by several orders of magnitudes will have serious implications for in silico safety assurance.

Another limitation of QSPR approach is that they do not consider the dynamic process of transdermal permeation, which is influenced by many other factors including the physical chemical properties of solutes. To model the dynamic events of transdermal permeation, many researchers proposed mechanistic models of transdermal permeation based on diffusion theory. Early studies attempt to use simple diffusion theory assuming the SC as homogenous media[11,19,20] and did not consider the heterogeneous structure of the skin. Simple diffusion models are not predictive as it is necessary to obtain the overall diffusivity of skin from experimental data,[21] although the overall diffusivity can be related to skin permeability. Besides, solute distribution in different phases of the SC can not be described by simple diffusion. Michaels et al.[22] first considered solute diffusion in the heterogeneous SC and proposed the so-called "brick-and-mortar" model where brick represents the transcellular corneocytes phase and mortar represents the intercellular lipid phase. The "brick-and-mortar" model soon received wide interest and was adopted by many researchers.[23–25] Using the "brick and mortar" model, major progress has been made in estimating the tortuosity of the intercellular lipid pathway of the SC. In particular, by using scaled particle diffusion theory and considering the tortuosity of SC lipids, Mitragotri[2,10] obtained a theoretical equation for predicting skin permeability. However, many reported "brick-and-mortar" models are still not fully predictive. Many studies assumed the corneocytes as impermeable barriers. Recently, Wang et al. presented a two-phase microscopic diffusion model which is similar to the "brick-and-mortar" model.[26,27] They first showed that some of the solute diffusion and partition properties in the SC lipid and corneocytes can be established separately by relating to the fundamental physicochemical properties of solute. Yet, one of the transport properties (transbilayer mass transfer coefficient, k_{trans}) is still empirically obtained by fitting to the simulated experimental data of skin permeability. Furthermore, Wang et al.[27] had limited consideration of hydrophilic solutes. The dataset they used to validate their model only included few hydrophilic solutes and the hydrophilic solute (sucrose, $\log K_{ow} = -3.7$) is excluded as an outlier. To our knowledge, the following challenges remain as far as in silico prediction of transdermal permeation is concerned: (i) quantification of the contribution of intercellular and transcellular pathways to transdermal permeation and absorption; (ii) determination of model parameters separately without fitting to the experimental data to be modeled; (iii) closed-form prediction of both skin permeability and the dynamic process of dermatopharmacokinetic absorption of solutes.

The present work attempts to address the aforementioned issues by adopting a recently published cellular structure and composition based mechanistic model for the closed-form prediction of transdermal permeation and dermatopharmacokinetic absorption of solutes.[28] A main advantage of the model is that the partition and diffusion properties of the SC lipid matrix and corneocytes are estimated separately by considering the heterogeneous nature of the SC. In this part of the article, the model has been applied to predict the skin permeability of a large data set of both hydrophobic and hydrophilic chemical compounds. Compared with previous models, the current model gives much improved prediction of skin permeability, in particular, for hydrophilic solutes and moderately hydrophobic solutes. Furthermore, contributions of the two pathways (intercellular lipid pathway and transcellular pathway) to skin permeability of both hydrophobic and hydrophilic permeants have been quantified. Apart from skin permeability, another important aspect of modeling transdermal permeation is the prediction of the dynamic absorption and bioavailability of topically administered solutes in vivo. This will be discussed in a separate article, Part II (Lian GP, Chen LJ, Pudney PDA, Mickael M, Han LJ. Submitted, AIChE J).

Methods

Model description

The "brick and mortar" model adopted here has been reported recently.[28] Detailed description of the model, including the geometric and compositional parameters as well as solute partition and diffusion properties of the SC lipids and corneocytes can be found in the original article.[28] Here, for completeness, a brief summary is given.

The geometrical and compositional parameters of the SC are set to typical values quoted in the literature (Table 1).[1,2] In particular, the SC thickness is consistent with that used

Table 1. Structural and Compositional Properties of SC for "Brick-and-Mortar" Model

Parameters	Value
Layers of corneocytes, N	16
Width of corneocytes, d	40 μm
Heigh of corneocytes, t	0.8 μm
Thickness of intercellular lipid, g	0.075 μm
The lateral spacing between keratinocytes, s	0.075 μm
The offset ratio, w	3 or 8
Dry mass fraction of lipid, f_l	12.5%
Dry mass fraction of keratin, f_k	87.5%
Saturated water content of the SC, f_{sc}	55% (w/w)
Density of water, ρ_w	1000 kg/m^3
Density of lipid, ρ_l	1000 kg/m^3
Density of keratin, ρ_k	1200 kg/m^3

Table 2. Eight Representative Solutes for Deriving Two Parameters (α and β) in Eq 5

Permeants	log K_{ow}	M_W (Da)	Observed log K_p (cm/s)	Predicted log K_p (cm/s)
Mannitol	−3.01	182.2	−8.16	−8.04
Water	−1.38	18	−6.32	−6.48
Methanol	−0.77	32	−6.56	−6.44
Hydrocortisone	1.61	362.5	−7.48	−7.36
Hexanol	2.03	102.2	−5.11	−5.42
Octanoic acid	3.05	144.2	−5.16	−5.13
Ibuprofen	3.97	206.3	−5.00	−5.02
Decanol	4.57	158.3	−4.30	−4.20

by Johnson et al.[1] Saturated water content was set to 55% (w/w) to match the in vivo data.[3,29] We are aware that higher SC thickness and other SC parameters (e.g., saturated water content) were used elsewhere.[26,27]

To obtain closed-form prediction, the partition and diffusion properties of the SC lipids and corneocytes need to be determined separately. Here, the solute partition between the SC lipids and water is calculated from the widely used correlation[2,10]

$$K_{mw} = K_{ow}^{0.7} \tag{1}$$

The corneocytes are considered as a porous media of gel phase and the partition coefficient between corneocytes and water is related to the hydration level by the following equation

$$K_{bw} = (1 - \phi_b)K_{kw} + \theta_b \tag{2}$$

where θ_b is the volume fraction of water in the corneocyte-phase, ϕ_b is the volume fraction of water at saturation for the corneocytes-phase, K_{kw} is the partition coefficient between keratin and water and can be calculated by the following equation[28,30]

$$K_{kw} = \begin{cases} 5.6{K_{ow}}^{0.27} & \text{if} \quad K_{ow} > 10 \\ \dfrac{1 + K_{ow}^{0.7}}{2} & \text{if} \quad K_{ow} \le 10 \end{cases} \tag{3}$$

The diffusion coefficient of a solute in the SC lipid phase, D_m, is calculated by the mechanism model developed by Mitragotri[2]

$$D_m(\mathrm{m}^2/\mathrm{s}) = 2 \times 10^{-9} \ \exp(-0.46{r_s}^2) \tag{4}$$

where r_s is the radius of solute (Å) and can be calculated by the empirical equation $4/3\pi{r_s}^3 = 0.9087\ M_W$.[31]

There have been very limited studies on solute diffusion in corneocytes and few experimental data are available. Kasting et al.[32] proposed a diffusion model of water in corneocytes based on water self-diffusion coefficient measured by nuclear magnetic resonance (NMR), but it does not applies to effective diffusion coefficient of solute in corneocytes. Here, as an approximation, the corneocytes are considered as a gel phase and the diffusion coefficient is related to the hydration level using the combined hydrodynamic/obstruction diffusion theory in gel networks as follows[33]

$$\frac{D_b}{D_w} = \frac{\exp[-\alpha S^{\lambda}]}{[1 + \frac{r_s}{\sqrt{k}} + \frac{r_s^2}{3k}]} \tag{5}$$

where

$$k = \beta {r_f}^2 (1 - \theta_b)^{\gamma} \tag{6}$$

$$S = (1 - \theta_b)\left(\frac{r_s + r_f}{r_f}\right)^2 \tag{7}$$

where D_w is the diffusion coefficient of solute in water and can be predicted using the Stokes–Einstein equation,[34] k is the hydraulic permeability and is estimated from the correlation derived by Jackson and James,[35] r_f is the radius of keratin microfibril ($r_f = 35$ Å),[32] α, λ, β, and γ are model parameters and their values are set to $\lambda = 1.09$, $\gamma = -1.17$, $\alpha = 9.47$, and $\beta = 9.32 \times 10^{-8}$. The values of λ and γ are the same as that in Johnson et al.[33] The values of α and β are obtained by applying the model to fit skin permeability data of eight representative solutes shown in Table 2. The relationship between D_b and M_W has been shown in Figure 1. For solutes of M_W between 50 Da and 1000 Da, D_b is predicted to be ranging from 6.6×10^{-15} m^2/s to 1.4×10^{-16} m^2/s. These predicted values compare well with those estimated by Heisig et al.,[24] where the predicted D_b value of molecular with $M_W = 300$ Da was about 1.2×10^{-15} m^2/s.

Computer simulation

More details on computer simulation have been described in our previous article.[28] Here, a brief summary is given. A fine mesh is used for numerical simulation in this study, with each corneocyte layer divided into 33 grids, giving a total number of $N_{grids} = 33N_{layers}$ grids. Using the numerical scheme of finite volume, the solute concentration of each grid satisfied the following mass conservation equation

$$\frac{dC_A}{dt} = -\frac{\sum_B q_{AB}}{V} \tag{8}$$

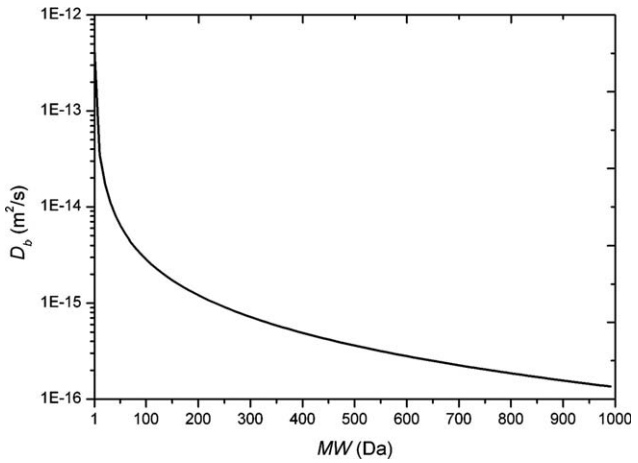

Figure 1. The relationship between solute diffusion coefficient in the corneocytes (D_b) and molecular weight (M_W).

with

$$q_{AB} = \frac{S_{AB}}{\frac{\delta_A}{D_A} + \frac{P_{AB}\delta_B}{D_B}}(C_A - P_{AB}C_B) \quad (9)$$

where C_A and C_B are the solute concentrations in grid A and B, V is the volume of grid A, t is time, and q_{AB} is the flux of solute from grid A to its neighboring grid B, S_{AB} is the interfacial area between grid A and grid B, D_A and D_B are the diffusion coefficients of grid A and B, δ_A and δ_B are the corresponding diffusion length, P_{AB} is the solute partition coefficient between grid A and B.

In total, there are N_{grids} ordinary differential equations (ODEs) of mass balance. The ODEs are solved using MATLAB solver ode15s with variable time steps. The solver is based on the backward differentiation formula, also known as Gear/s method for stiff ordinary differential equations. For predicting skin permeability (K_p), infinite source and infinite sink are assumed for the upper and lower boundaries. The concentrations of the simulated chemicals in the vehicle (C_v) are all set to unity. The computer simulation proceeds until reaching steady state, at which the skin permeability (K_p) is obtained from steady state flux (J_{ss}). Under the simulated infinite source and infinite sink condition, the equation for deriving the skin permeability K_p is as follows

$$K_p = \frac{J_{ss}}{C_v} \quad (10)$$

Model evaluation

Here, we apply our model to predict skin permeability and compare with the measured data of the 127 chemical compounds compiled from various sources (Table 3).[1,13,17,36–39] Prediction of the current model is compared with other models. The parameters used to evaluate the performance of each model are: R^2 (correlation coefficient between predicted and observed values) and MSE (mean squared error).

$$R^2 = 1 - \frac{\sum_{i=1}^{n}(Y_i^{obs} - Y_i^{pre})^2}{\sum_{i=1}^{n}(Y_i^{obs} - \overline{Y}^{obs})^2} \quad (11)$$

$$MSE = \frac{\sum_{i=1}^{n}(Y_i^{obs} - Y_i^{pre})^2}{n} \quad (12)$$

where Y_i^{obs} and Y_i^{pre} are the observed and predicted log K_p values, $\overline{Y}^{obs}$ is the mean value of the observed log K_p values, n is the sample number.

Results and Discussion

The effect of off-set ratio on skin permeability

With the "brick-and-mortar" model, the off-set ratio, w, is expressed as the ratio to the two horizontal diffusion lengths of solute from the inter-keratinocyte lipid of the upper layer to the inter-keratinocyte lipid of the next lower layer. There have been some inconsistencies in quoting the off-set ratio, w. In some modeling studies, it is set to 8.[1,2] Others argued that this is the typical value for rodent skin and for human skin the typical value of the off-set ratio is 3.[40] The off-set ratio, w, affects the effective length of the intercellular lipid pathway. When $w = 0$, or ∞, the inter-keratinocyte of each corneocyte layer is vertically aligned and solute diffusion in the lipid matrix has the shortest pathway. At $w = 1$, the lipid diffusion pathway is the longest. The equation for the effective length of the tortuous lipid pathway, L_e, was previously given as[42]

$$L_e = \left[1 + \frac{d}{(1+w)(\frac{Nt}{N-1} + g)}\right] \times L_{sc} \quad (13)$$

where L_{sc} is the thickness of the SC.

When other geometrical parameters are kept to the same, the value of L_e for $w = 3$ is about two times higher than that when $w = 8$. For highly hydrophobic solutes of which the main permeation pathway is through the intercellular lipid route, such a difference in L_e contributes to a maximum shift of 0.3 in the log K_p values. For solutes of which the permeation pathway is through both intercellular lipid and transcellular route, such a difference in L_e has less effect on the predicted skin permeability. We performed computer simulations with two scenarios of $w = 3$ and $w = 8$. For highly hydrophilic solutes, the two scenarios ($w = 3$ and $w = 8$) gave almost the same prediction of K_p values ($R^2 =$ 0.53, 0.53 and MSE = 0.25, 0.25, respectively). Overall, the two scenarios of $w = 3$ and $w = 8$ gave similar prediction accuracy as measured by R^2 (0.67, 0.74) and MSE (0.37, 0.29). Slightly better prediction is achieved for $w = 8$ and hence this is the set value in the following analysis. This is also the off-set ratio used by many recent studies for estimating the lipid pathway tortuousity of the human SC.

Model comparisons

In recent study,[18] we have shown that the simple QSPR model of Potts & Guy[11] and the mechanistic model of Mitragotri[10] gave the best prediction. Other QSPR models fail to give satisfactory prediction of skin permeability for the comprehensive data sets of 127 chemicals. We have also shown that the two best models under-predict skin permeability of hydrophilic solutes by several orders of magnitudes. Here, we compare our model prediction with the two best models and two other recently reported models.[17,26,27] The model of Abraham & Martins[17] is an improved version of their earlier QSPR models correlating skin permeability to the molecular structure-level descriptors of free energy.[6,7] The model of Wang et al.[26,27] considered both the intercellular and transcellular pathways assuming convoluted and perfect lipid bilayers around the corneocytes.

The R^2 and MSE of the respective models are listed in Table 4. Clearly, for the whole dataset the current model gave the best prediction with $R^2 = 0.74$ and MSE = 0.29. Mitrogotri model[10] gave the second best prediction, with $R^2 =$ 0.58 and MSE = 0.46. Potts & Guy[11] and Wang et al.[27] model give the similar prediction accuracy ($R^2 = 0.52$ and $MSE = 0.53$ for Potts & Guy,[11] $R^2 = 0.53$ and MSE = 0.53 for Wang et al.[27] model). The late improved Abraham & Martins model still gave unsatisfactory prediction with R^2

Table 3. List of Chemical Compounds and Measured Skin Permeability

Solute	Log K_{ow}	M_W	Measured log Kp (cm/s) Value	Reference	Potts & Guy[11]	Predicted log K_p (cm/s) Abraham et al.[17]	Mitragotri[10]	Wang et al.[27]	Current Model ($w = 8$)
Sucrose	−3.70	342.30	−8.84	38	−11.02	−12.70	−11.40	−11.54	−8.43
Aspartic acid	−3.47	133.10	−7.43	37	−9.58	−8.36	−9.59	−9.94	−7.88
Lysine	−3.05	146.20	−6.87	37	−9.36	−8.17	−9.42	−9.72	−7.92
Mannitol	−3.01	182.17	−8.51	39	−9.55	−9.85	−9.71	−10.00	−8.04
Mannitol	−3.01	182.17	−8.18	39	−9.55	−9.85	9.71	−10.00	−8.04
Mannitol	−3.01	182.17	−8.16	39	−9.55	−9.85	−9.71	−10.00	−8.04
Mannitol	−3.01	182.17	−7.92	39	−9.55	−9.85	−9.71	−10.00	−8.04
Mannitol	−3.01	182.17	−7.77	39	−9.55	−9.85	−9.71	−10.00	−8.04
Histidine	−2.90	155.20	−7.82	37	−9.31	−8.52	−9.40	−9.68	−7.95
Urea	−2.11	60.60	−7.39	36	−8.17	−8.24	−7.87	−7.91	−7.30
Ouabain	−2.00	584.60	−9.66	38	−11.29	−12.68	−10.51	−10.93	−8.72
Water	−1.38	18.00	−7.26	1	−7.39	−6.69	−6.75	−6.27	−6.48
Water	−1.38	18.00	−7.08	1	−7.39	−6.69	−6.75	−6.27	−6.48
Water	−1.38	18.00	−6.86	1	−7.39	−6.69	−6.75	−6.27	−6.48
Water	−1.38	18.00	−6.56	1	−7.39	−6.69	−6.75	−6.27	−6.48
Water	−1.38	18.00	−6.41	13	−7.39	−6.69	−6.75	−6.27	−6.48
Water	−1.38	18.00	−6.37	13	−7.39	−6.69	−6.75	−6.27	−6.48
Water	−1.38	18.00	−6.36	39	−7.39	−6.69	−6.75	−6.27	−6.48
Water	−1.38	18.00	−6.36	39	−7.39	−6.69	−6.75	−6.27	−6.48
Water	−1.38	18.00	−6.32	39	−7.39	−6.69	−6.75	−6.27	−6.48
Water	−1.38	18.01	−6.80	39	−7.39	−6.69	−6.75	−6.27	−6.48
Water	−1.38	18.01	−6.72	39	−7.39	−6.69	−6.75	−6.27	−6.48
Water	−1.38	18.01	−6.71	39	−7.39	−6.69	−6.75	−6.27	−6.48
Water	−1.38	18.01	−6.68	1	−7.39	−6.69	−6.75	−6.27	−6.48
Water	−1.38	18.01	−6.60	1	−7.39	−6.69	−6.75	−6.27	−6.48
Water	−1.38	18.01	−6.48	1	−7.39	−6.69	−6.75	−6.27	−6.48
Water	−1.38	18.01	−6.43	39	−7.39	−6.69	−6.75	−6.27	−6.48
Water	−1.38	18.01	−6.42	1	−7.39	−6.69	−6.75	−6.27	−6.48
n-Nitrosodiethanolamine	−1.28	134.13	−8.30	1	−8.03	−7.84	−8.07	−8.17	−7.64
2,3-Butanediol	−0.92	90.12	−7.47	17	−7.50	−6.19	−7.38	−7.39	−7.18
2,3-Butanediol	−0.92	90.12	−7.86	1	−7.50	−6.19	−7.38	−7.39	−7.18
5-Fluorouracil	−0.89	130.08	−6.82	17	−7.73	−7.46	−7.76	−7.82	−7.48
Methanol	−0.77	32.00	−6.38	17	−7.04	−6.57	−6.55	−6.22	−6.44
Methanol	−0.77	32.00	−6.56	39	−7.04	−6.57	−6.55	−6.22	−6.44
Methanol	−0.77	32.04	−6.35	13	−7.04	−6.57	−6.55	−6.23	−6.44
2-Ethoxyethanol	−0.32	90.10	−6.68	17	−7.08	−5.87	−6.96	−6.90	−6.87
Ethanol	−0.31	46.07	−7.06	1	−6.80	−6.23	−6.43	−6.18	−6.37
Ethanol	−0.31	46.10	−6.17	17	−6.80	−6.23	−6.43	−6.18	−6.37
Ethanol	−0.31	46.10	−6.56	39	−6.80	−6.23	−6.43	−6.18	−6.37
p-Phenylenediamine	−0.30	108.10	−6.98	17	−7.17	−6.59	−7.13	−7.10	−7.02
Boric Acid	−0.22	61.83	−7.48	39	−6.83	−7.98	−6.57	−6.40	−6.51
Boric Acid	−0.22	61.83	−7.09	39	−6.83	−7.98	−6.57	−6.40	−6.51
Boric Acid	−0.22	61.83	−6.86	39	−6.83	−7.98	−6.57	−6.40	−6.51
Caffeine	−0.07	194.00	−7.08	17	−7.53	−7.07	−7.75	−7.71	−7.54
Caffeine	−0.07	194.20	−7.14	1	−7.53	−7.07	−7.75	−7.71	−7.54
Caffeine	−0.07	194.20	−6.35	39	−7.53	−7.07	−7.75	−7.71	−7.54
o-Phenylenediamine	0.15	108.10	−6.70	17	−6.85	−6.47	−6.82	−6.74	−6.75
Propanol	0.25	60.10	−6.48	38	−6.49	−5.91	−6.22	−5.99	−6.19
Propanol	0.25	60.10	−5.91	17	−6.49	−5.91	−6.22	−5.99	−6.18
Propanol	0.25	60.10	−6.33	1	−6.49	−5.91	−6.22	−5.99	−6.18
2-Butanone	0.29	72.11	−5.90	1	−6.53	−5.91	−6.33	−6.15	−6.29
Nicotinic Acid	0.36	123.11	−8.18	39	−6.80	−6.50	−6.82	−6.73	−6.75
Diethylcarbamazine	0.37	199.30	−7.45	38	−7.25	−6.80	−7.49	−7.40	−7.33
Nicorandil	0.43	211.18	−7.13	39	−7.28	−8.73	−7.54	−7.43	−7.37
2-nitro p-phenylenediamine	0.53	153.10	−6.66	17	−6.86	−6.32	−6.98	−6.89	−6.89
Barbital	0.65	184.20	−7.51	1	−6.96	−6.89	−7.16	−7.05	−7.05
Dimethylethylamine	0.70	73.14	−6.26	39	−6.25	−5.43	−6.06	−5.84	−6.03
Dimethylethylamine	0.70	73.14	−5.95	39	−6.25	−5.43	−6.06	−5.84	−6.03
Butyric acid	0.79	88.11	−6.56	38	−6.28	−5.37	−6.16	−5.97	−6.13
Resorcinol	0.80	110.10	−6.70	17	−6.40	−6.22	−6.38	−6.24	−6.34
Methyl nicotinate	0.83	137.14	−6.07	39	−6.55	−5.80	−6.62	−6.50	−6.56
Methyl nicotinate	0.83	137.14	−6.02	39	−6.55	−5.80	−6.62	−6.50	−6.56
Methyl nicotinate	0.83	137.14	−5.97	39	−6.55	−5.80	−6.62	−6.50	−6.56
4-chloro-4-phenylenediamine	0.85	142.60	−6.54	17	−6.57	−6.17	−6.66	−6.53	−6.60
Butanol	0.88	74.10	−6.21	1	−6.13	−5.59	−5.94	−5.70	−5.92

Table 3. (Continued)

Solute	Log K_{ow}	M_W	Measured log Kp (cm/s) Value	Reference	Potts & Guy[11]	Predicted log K_p (cm/s) Abraham et al.[17]	Mitragotri[10]	Wang et al.[27]	Current Model ($w = 8$)
Butanol	0.88	74.10	−6.08	1	−6.13	−5.59	−5.94	−5.70	−5.92
Butanol	0.88	74.14	−5.70	17	−6.13	−5.59	−5.94	−5.70	−5.92
Ethylether	0.89	74.10	−5.36	1	−6.12	−5.22	−5.93	−5.70	−5.91
Morphine	0.89	285.30	−7.81	1	−7.41	−7.32	−7.79	−7.53	−7.50
Aniline	0.90	93.10	−5.21	36	−6.23	−5.46	−6.14	−5.95	−6.11
Dihydromorphine	0.93	287.36	−8.38	36	−7.39	−5.98	−7.77	−7.51	−7.49
4-amino-2-nitrophenol	0.96	154.10	−6.11	36	−6.56	−5.99	−6.69	−6.55	−6.62
Scopolamine	0.98	303.40	−7.86	1	−7.45	−7.22	−7.85	−7.55	−7.53
Aldosterone	1.08	360.40	−7.86	1	−7.73	−7.00	−8.18	−7.75	−7.69
Aldosterone	1.08	360.40	−7.79	1	−7.73	−7.00	−8.18	−7.75	−7.69
Benzyl alcohol	1.10	108.10	−5.78	1	−6.18	−5.68	−6.15	−5.97	−6.12
Benzyl alcohol	1.10	108.10	−5.33	38	−6.18	−5.68	−6.15	−5.97	−6.12
Ephedrine	1.13	165.20	−5.78	1	−6.51	−6.21	−6.66	−6.51	−6.59
Nicotine	1.17	162.23	−6.04	39	−6.46	−6.05	−6.61	−6.45	−6.54
Nicotine	1.17	162.23	−5.54	1	−6.46	−6.05	−6.61	−6.45	−6.54
Nicotine	1.17	162.30	−5.28	39	−6.46	−6.05	−6.61	−6.45	−6.54
Acetylsalicylic Acid	1.19	180.16	−5.70	39	−6.55	−5.81	−6.75	−6.58	−6.67
Codeine	1.19	299.40	−7.09	1	−7.28	−6.97	−7.68	−7.36	−7.38
2-Amino-4-Nitrophenol	1.26	154.10	−6.74	36	−6.35	−5.86	−6.48	−6.31	−6.41
Ethyl nicotinate	1.32	151.17	−5.77	39	−6.28	−5.55	−6.41	−6.23	−6.35
Ethyl nicotinate	1.32	151.17	−5.74	39	−6.28	−5.55	−6.41	−6.23	−6.35
2-Phenylethanol	1.36	122.20	−5.44	1	−6.08	−5.59	−6.11	−5.91	−6.07
Pentanoic acid	1.39	102.13	−6.26	39	−5.94	−5.33	−5.89	−5.66	−5.86
Coumarin	1.39	146.15	−5.60	39	−6.20	−5.12	−6.31	−6.13	−6.26
Coumarin	1.39	146.15	−5.46	38	−6.20	−5.12	−6.31	−6.13	−6.26
Hydrocortisone succinamate	1.43	461.60	−8.14	1	−8.10	−7.58	−8.11	−7.85	−7.63
Phenol	1.46	94.10	−5.64	13	−5.84	−5.34	−5.75	−5.51	−5.73
Phenol	1.46	94.10	−5.44	1	−5.84	−5.34	−5.75	−5.51	−5.73
Phenol	1.46	94.10	−5.27	1	−5.84	−5.34	−5.75	−5.51	−5.73
Phenobarbital	1.47	232.20	−6.89	1	−6.67	−6.66	−6.98	−6.74	−6.83
Benzaldehyde	1.48	106.10	−4.77	1	−5.90	−5.15	−5.86	−5.64	−5.83
Benzaldehyde	1.48	106.10	−4.41	36	−5.90	−5.15	−5.86	−5.64	−5.84
Pentanol	1.51	88.20	−5.78	1	−5.77	−5.26	−5.66	−5.39	−5.63
Hydromorphone	1.60	285.30	−7.63	1	−6.90	−7.05	−7.29	−6.95	−7.04
Hydrocortisone	1.61	362.50	−8.35	1	−7.37	−6.90	−7.82	−7.33	−7.36
Hydrocortisone	1.61	362.50	−7.48	1	−7.37	−6.90	−7.82	−7.33	−7.36
Hydrocortisone	1.61	362.50	−7.19	1	−7.37	−6.90	−7.82	−7.33	−7.36
Nitroglycerine	1.62	227.09	−5.51	38	−6.54	−6.87	−6.83	−6.58	−6.70
Butobarbital	1.73	212.40	−7.27	1	−6.37	−6.25	−6.64	−6.39	−6.53
Atropine	1.83	289.38	−7.68	39	−6.77	−6.37	−7.16	−6.79	−6.93
Dexamethasone	1.83	392.50	−7.75	1	−7.39	−6.71	−7.83	−7.28	−7.34
Digitoxin	1.85	764.92	−8.44	38	−9.65	−8.25	−7.81	−8.04	−7.55
Benzoic Acid	1.87	122.10	−5.16	39	−5.72	−5.27	−5.75	−5.50	−5.72
Hydrocortisone hemisuccinate	1.89	462.50	−6.76	1	−7.78	−7.18	−7.78	−7.48	−7.37
4-Nitrophenol	1.91	139.10	−5.81	1	−5.79	−5.34	−5.88	−5.64	−5.85
Hexanoic acid	1.92	116.16	−5.41	38	−5.65	−5.00	−5.66	−5.40	−5.63
p-Cresol	1.94	108.10	−5.31	1	−5.58	−5.75	−5.56	−5.29	−5.54
Corticosterone	1.94	346.50	−7.56	1	−7.04	−6.04	−7.48	−6.99	−7.14
Corticosterone	1.94	346.50	−7.08	1	−7.04	−6.04	−7.48	−6.99	−7.14
Corticosterone	1.94	346.50	−6.81	1	−7.04	−6.04	−7.48	−6.99	−7.14
o-Cresol	1.95	108.10	−5.36	1	−5.57	−5.22	−5.56	−5.28	−5.54
m-Cresol	1.96	108.10	−5.38	1	−5.57	−5.22	−5.55	−5.27	−5.53
Methylhydroxybenzoate	1.96	152.10	−5.60	1	−5.84	−5.25	−5.97	−5.72	−5.93
Trichloromethane	1.97	119.38	−5.35	39	−5.63	−4.33	−5.65	−5.39	−5.63
3-Nitrophenol	2.00	139.11	−5.81	1	−5.73	−5.16	−5.82	−5.57	−5.79
Hexanol	2.03	102.20	−5.44	1	−5.48	−4.94	−5.44	−5.15	−5.42
Hexanol	2.03	102.20	−5.26	1	−5.48	−4.94	−5.44	−5.15	−5.42
Hexanol	2.03	102.20	−5.11	1	−5.48	−4.94	−5.44	−5.15	−5.42
Hydrocortisone *N*,*N*-dimethylsuccinamate	2.03	489.60	−7.72	1	−7.85	−6.88	−7.69	−7.44	−7.33
Amylobarbital	2.07	226.30	−6.20	1	−6.21	−6.01	−6.51	−6.21	−6.42
Isoquinoline	2.08	129.20	−5.33	1	−5.61	−5.25	−5.67	−5.40	−5.65
Anisole	2.11	108.10	−4.69	1	−5.46	−4.75	−5.44	−5.15	−5.43
Benzene	2.13	78.10	−4.51	1	−5.26	−4.53	−5.11	−4.75	−5.10
Benzene	2.13	78.10	−4.35	1	−5.26	−4.53	−5.11	−4.75	−5.10
2-Chlorophenol	2.15	128.60	−5.04	1	−5.56	−4.95	−5.62	−5.34	−5.59

Table 3. (Continued)

Solute	Log K_{ow}	M_W	Measured log Kp (cm/s)			Predicted log K_p (cm/s)			
			Value	Reference	Potts & Guy[11]	Abraham et al.[17]	Mitragotri[10]	Wang et al.[27]	Current Model ($w = 8$)
Griseofulvin	2.18	352.77	−6.44	39	−6.90	−5.96	−7.36	−6.82	−7.05
Griseofulvin	2.18	352.77	−6.27	39	−6.90	−5.96	−7.36	−6.82	−7.05
Salicyclic acid	2.26	138.10	−5.76	39	−5.54	−5.30	−5.63	−5.35	−5.61
Salicyclic acid	2.26	138.10	−5.07	1	−5.54	−5.30	−5.63	−5.35	−5.61
Salicyclic acid	2.26	138.12	−5.48	39	−5.54	−5.30	−5.63	−5.35	−5.61
Salicyclic acid	2.26	138.12	−5.44	39	−5.54	−5.30	−5.63	−5.35	−5.61
Salicyclic acid	2.26	138.12	−5.42	1	−5.54	−5.30	−5.63	−5.35	−5.61
Butyl nicotinate	2.27	179.22	−5.34	39	−5.78	−4.94	−5.99	−5.70	−5.95
3,4-xylenol	2.30	122.10	−5.00	1	−5.41	−4.87	−5.45	−5.15	−5.43
Hydrocortisone pimelamate	2.30	503.64	−6.61	1	−7.74	−6.64	−7.50	−7.26	−7.21
Heptanol	2.31	116.20	−5.05	1	−5.37	−4.61	−5.38	−5.08	−5.37
Heptanol	2.31	116.20	−4.98	1	−5.37	−4.61	−5.38	−5.08	−5.37
4-Chlorophenol	2.39	128.56	−5.00	1	−5.39	−4.89	−5.45	−5.15	−5.43
Benzyl nicotinate	2.40	213.24	−5.35	39	−5.90	−5.03	−6.18	−5.85	−6.12
Heptanoic acid	2.42	130.19	−5.26	38	−5.38	−4.67	−5.44	−5.14	−5.43
Lidocaine	2.44	234.30	−5.96	1	−6.00	−5.20	−6.32	−5.96	−6.25
1,1,1-Trichloroethane	2.49	133.40	−5.90	36	−5.35	−4.19	−5.42	−5.12	−5.41
4-Ethylphenol	2.58	122.20	−5.02	1	−5.21	−5.02	−5.25	−4.93	−5.24
4-Bromophenol	2.59	173.01	−5.00	1	−5.52	−4.83	−5.71	−5.39	−5.69
Hydrocortisone methylsuccinate	2.60	476.57	−7.23	1	−7.36	−6.20	−7.29	−6.95	−7.05
2-Naphthol	2.70	144.20	−5.15	1	−5.26	−5.13	−5.38	−5.05	−5.36
2-Naphthol	2.70	144.20	−5.11	1	−5.26	−5.13	−5.38	−5.05	−5.36
Meperidine	2.72	247.40	−5.99	38	−5.88	−5.18	−6.22	−5.82	−6.16
Toluene	2.73	92.14	−3.56	1	−4.92	−4.18	−4.84	−4.46	−4.84
Etorphine	2.79	411.50	−6.00	38	−6.83	−6.11	−7.15	−6.57	−6.91
Hydrocortisone hydroxyhexanoate	2.79	476.60	−6.60	1	−7.23	−5.88	−7.15	−6.79	−6.95
Hydrocortisone propinate	2.80	418.50	−6.02	1	−6.86	−5.80	−7.15	−6.59	−6.91
Styrene	2.95	104.10	−3.74	1	−4.84	−4.15	−4.82	−4.43	−4.81
Octanol	3.00	130.20	−4.84	1	−4.96	−4.29	−5.04	−4.68	−5.03
Octanol	3.00	130.20	−4.51	1	−4.96	−4.29	−5.04	−4.68	−5.03
Octanol	3.00	130.23	−4.77	39	−4.96	−4.29	−5.04	−4.68	−5.03
Octanoic acid	3.05	144.21	−5.16	38	−5.01	−4.35	−5.13	−4.77	−5.13
2,4-Dichlorophenol	3.06	163.00	−4.78	1	−5.12	−4.55	−5.29	−4.93	−5.28
Piroxicam	3.06	331.40	−7.37	36	−6.15	−8.71	−6.60	−6.01	−6.48
4-Chlorocresol	3.10	142.58	−4.82	1	−4.97	−5.05	−5.08	−4.72	−5.08
Ethyl benzene	3.15	106.17	−3.48	1	−4.71	−3.86	−4.70	−4.30	−4.70
Naproxen	3.18	230.27	−6.10	38	−5.45	−4.72	−5.77	−5.34	−5.74
Naproxen	3.18	230.30	−6.95	39	−5.45	−4.72	−5.77	−5.34	−5.74
Naproxen	3.18	230.30	−4.97	1	−5.45	−4.72	−5.77	−5.34	−5.74
Fluocinonide	3.19	494.60	−6.33	1	−7.05	−6.08	−6.87	−6.52	−6.73
Hydrocortisone hemipimelate	3.26	503.60	−6.30	1	−7.06	−5.87	−6.83	−6.49	−6.70
Chloroxylenol	3.27	156.60	−4.83	1	−4.93	−4.70	−5.09	−4.71	−5.09
Thymol	3.30	150.20	−4.84	1	−4.87	−4.31	−5.01	−4.63	−5.01
Testosterone	3.32	288.40	−6.21	1	−5.70	−5.06	−6.11	−5.58	−6.05
Testosterone	3.32	288.40	−5.83	1	−5.70	−5.06	−6.11	−5.58	−6.05
Testosterone	3.32	288.40	−5.48	39	−5.70	−5.06	−6.11	−5.58	−6.05
Testosterone	3.32	288.40	−4.95	39	−5.70	−5.06	−6.11	−5.58	−6.05
Chlorpheniramine	3.38	274.80	−6.22	38	−5.58	−5.19	−5.97	−5.45	−5.92
Propranolol	3.48	257.34	−6.48	39	−5.40	−5.58	−5.77	−5.27	−5.74
Propranolol	3.48	257.34	−6.33	39	−5.40	−5.58	−5.77	−5.27	−5.74
N-Hexyl Nicotinate	3.51	207.27	−5.30	39	−5.07	−4.33	−5.35	−4.92	−5.34
2,4,6-Trichlorophenol	3.69	197.50	−4.78	1	−4.88	−4.06	−5.15	−4.70	−5.14
Hydrocortisone methylpimelate	3.70	518.65	−5.82	1	−6.84	−5.27	−6.52	−6.17	−6.44
Nonanol	3.77	144.30	−4.78	1	−4.50	−3.96	−4.63	−4.20	−4.63
Progesterone	3.87	314.50	−5.43	1	−5.47	−4.54	−5.91	−5.27	−5.87
Progesterone	3.87	314.50	−5.08	1	−5.47	−4.54	−5.91	−5.27	−5.87
Sufentanil	3.95	386.60	−5.48	1	−5.85	−5.34	−6.34	−5.54	−6.25
Ibuprofen	3.97	206.28	−5.00	39	−4.74	−4.41	−5.02	−4.54	−5.02
Estradiol	4.01	272.40	−6.08	1	−5.11	−5.11	−5.51	−4.93	−5.49
Estradiol	4.01	272.40	−6.05	1	−5.11	−5.11	−5.51	−4.93	−5.49
Estradiol	4.01	272.40	−6.02	1	−5.11	−5.11	−5.51	−4.93	−5.49
Estradiol	4.01	272.40	−6.01	1	−5.11	−5.11	−5.51	−4.93	−5.49
Estradiol	4.01	272.40	−5.97	1	−5.11	−5.11	−5.51	−4.93	−5.49
Estradiol	4.01	272.40	−5.95	1	−5.11	−5.11	−5.51	−4.93	−5.49
Estradiol	4.01	272.40	−5.94	1	−5.11	−5.11	−5.51	−4.93	−5.49
Estradiol	4.01	272.40	−5.94	1	−5.11	−5.11	−5.51	−4.93	−5.49

Table 3. (Continued)

Solute	Log K_{ow}	M_W	Measured log Kp (cm/s)		Predicted log K_p (cm/s)				
			Value	Reference	Potts & Guy[11]	Abraham et al.[17]	Mitragotri[10]	Wang et al.[27]	Current Model ($w = 8$)
Estradiol	4.01	272.40	−5.84	1	−5.11	−5.11	−5.51	−4.93	−5.49
Estradiol	4.01	272.40	−5.82	1	−5.11	−5.11	−5.51	−4.93	−5.49
Estradiol	4.01	272.40	−5.77	1	−5.11	−5.11	−5.51	−4.93	−5.49
Fentanyl	4.05	336.50	−5.81	1	−5.48	−5.36	−5.94	−5.24	−5.89
Fentanyl	4.05	336.50	−5.56	38	−5.48	−5.36	−5.94	−5.24	−5.89
Indomethacin	4.27	357.80	−5.39	1	−5.45	−5.47	−5.93	−5.16	−5.88
Hydrocortisone hexanoate	4.48	460.60	−5.30	1	−5.93	−4.87	−5.97	−5.37	−5.93
Diclofenac	4.51	296.16	−6.56	39	−4.90	−4.77	−5.33	−4.67	−5.32
Diclofenac	4.51	296.16	−5.30	1	−4.90	−4.77	−5.33	−4.67	−5.32
Decanol	4.57	158.30	−4.65	1	−4.02	−3.64	−4.20	−3.73	−4.20
Decanol	4.57	158.30	−4.30	1	−4.02	−3.64	−4.20	−3.73	−4.20
Hydrocortisone octanoate	5.49	488.70	−4.76	1	−5.38	−4.25	−5.26	−4.65	−5.26

$= 0.42$ and MSE $= 0.64$. Figure 2 compares the prediction of the current model with the best QSPR model of Potts and Guy[11] and the mechanistic model of Mitragotri.[10] Much of the improvement in the predicted skin permeability of our model is from the hydrophilic solutes, as shown in Table 3. For hydrophilic solutes ($\log K_{ow} \leq -2$), all the other four models under-predict the skin permeability by 1–3 orders of magnitudes and the under-prediction generally increased with the increase in the hydrophilicity of the solutes (Figure 3). The under-prediction of hydrophilic solutes by both Potts & Guy[11] and Mitragotri[10] models has been already pointed out earlier.[18] A main drawback of many previous models, including the QSPR models, is that the contribution of the transcellular pathway to skin permeability has been ignored. Although Wang et al.[27] considered both the intercellular and transcellular pathways, their model still fails to give satisfactory prediction of the skin permeability of hydrophilic solutes. This is not surprising because they did not attempt to establish the diffusion properties of the corneocytes. Instead, they fitted the mass transfer property of the corneocytes using the modeled skin permeability data, which unfortunately, did not contain much hydrophilic solutes.

There are few modeling studies on transdermal permeation on hydrophilic solutes. For instance, Mitragotri[2] proposed four permeation pathways including free-volume diffusion through lipid bilayers, lateral diffusion along lipid bilayers, diffusion through aqueous pores, and diffusion through shunts. Compared with the early analytical model, inclusion of aqueous pores (in lipid matrix) and shunts improved the prediction for hydrophilic solutes. Still, there is still some significant under-prediction.

One may argue that accurate prediction of skin permeability of hydrophilic drugs is not very relevant because transdermal permeation of hydrophilic solutes is generally rather slow. However, for safety assurance of sensitizing chemicals, this is not necessary the case. Under-prediction of skin permeability by orders of magnitude will have serious implications. In addition, as we will show later, even for moderately hydrophobic solutes, the transcellular route through corneocytes can still contribute up to 25–75% of the total skin permeability.

Contribution of transcellular permeation pathway

To further examine the effect of the transcellular pathway on transdermal permeation, computer simulations have been carried out for two scenarios: the diffusion coefficient of the corneocyte set to $D_b \neq 0$ and $D_b = 0$, respectively. In the case of $D_b \neq 0$, the transcellular pathway through corneocytes is included. When D_b is set to zero, the widely used lipid pathway assumption is recovered. The relative contributions of the intercellular lipids pathway and transcellular pathway to the total skin permeability can be calculated as

$$CP_I = \frac{K_{p(D_b=0)}}{K_{p(D_b\neq 0)}} \times 100\% \tag{14}$$

$$CP_T = \frac{K_{p(D_b\neq 0)} - K_{p(D_b=0)}}{K_{p(D_b\neq 0)}} \times 100\% \tag{15}$$

The relative contribution of the two pathways to the overall skin permeability depends on the molecular weight and lipophilicity. The effect can be mapped into five regions in the $\log K_{ow} - M_W$ space as shown in Figure 4. In region I, the transcellular pathway dominates, contributing to more than 95% of the total skin permeability. The contribution of the tortuous lipid pathway in the region is negligibly small (less then 5%). Molecules in the region is generally highly hydrophilic ($\log K_{ow} < -2$) and about a handful molecules in the dataset fall into the region. In region II of the $\log K_{ow} - M_W$ space, the transcellular pathway still dominates, contributing to 75–95% of the total skin permeability and the contribution from the tortuous lipid pathway is still relatively small, of 5–25%. However, no molecules from the dataset fall

Table 4. Comparison of Skin Permeability Models: Coefficient of Determination (R^2) and Mean Absolute Error (MSE) Between Predicted Results and Measured Data

Models	Coefficient of Determination (R^2)	Mean Absolute Error (MSE)
Potts & Guy[11]	0.52	0.53
Abraham & Martins[17]	0.42	0.64
Mitragotri[10]	0.58	0.46
Wang et al.[27]	0.53	0.53
Current model ($w = 8$)	0.74	0.29

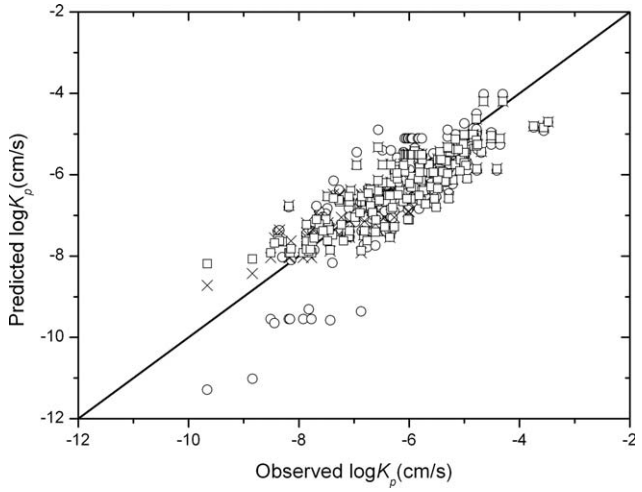

Figure 2. Comparison of observed and predicted skin permeability by Potts & Guy (○), Mitragotri (□), and current models (×).

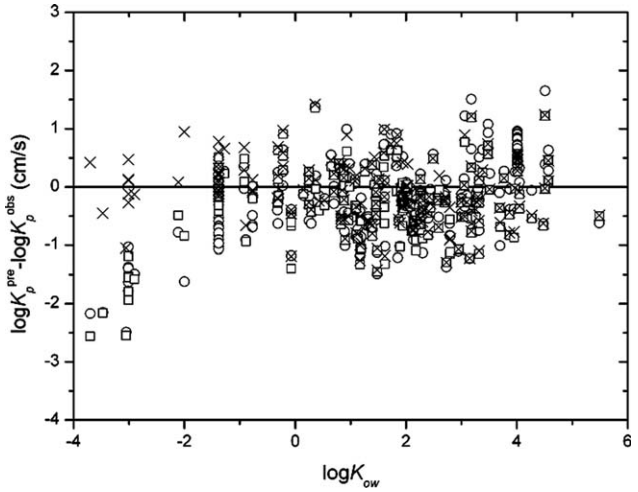

Figure 3. Comparison of predicted errors of skin permeability by Potts & Guy (○), Mitragotri (□), and current models (×).

into the region. The next region is the region where both the tortuous lipid pathway and the transcellular pathway are both important ($25\% \leq \mathrm{CP_I} \leq 75\%$). More than a quarter of the molecules from the dataset are in the region. Molecules in the region include both moderately hydrophilic (e.g., water) and moderately hydrophobic (e.g., aldosterone) and the corresponding log K_{ow} varied between -2 and 3. Further on the right of the log $K_{ow} - M_W$ map is region IV, where the tortuous intercellular lipid pathway is the main route of transdermal permeation, constitution 75–95% of the total skin permeability. The contribution from the transcellular pathway is very small. About half molecules from the dataset fall into the region. Most molecules in the region are hydrophobic but few are hydrophilic. Ethanol is in this region. On the far right on the log $K_{ow} - M_W$ map is region V. This is the region that the intercellular lipid pathway dominates, constituting to more than 95% of the total skin permeability. There are not many molecules (ca. 20) in the data set fall into the region. Molecules in the region are highly hydrophobic (log $K_{ow} > 2$).

It should be pointed out that the current simulation assumes that the SC is fully hydrated. Water consists of about 55–65% mass fraction of saturated SC and mainly exists in the corneocyte phase.[41] The hydration level of the SC depends on a number of factors including age, sex, ethnic groups, and environmental relative humidity.[41] It normally varies from ca. 15% at the top layer to ca. 55% near to the basal layer of the SC.[42] As the hydration level varies, the effective diffusion of solutes in the corneocytes is affected. It is shown that even for the moderately hydrophobic solutes the transcellular pathway can still contribute to 25–75% of the skin permeability. Thus, for hydrophilic solutes and moderately hydrophobic solutes in Region I and III, the interplay of skin hydration with environmental conditions is expected to have significant impact on their transdermal permeation. For instance, aldosterone is a moderately hydrophobic molecule (log $K_{ow} = 1.08$). If the SC is hydrated to 55% moisture content, the predicted skin permeability would be 2.04e-8 cm/s. This compares to a predicted skin permeability of 7.10e -9 cm/s (of 1/3 less) if the moisture content of SC is at normal condition varying from ca. 15% at the top to 55% near to the basal layer.

Conclusions

Transdermal permeation of solute through human SC depends not only on its cellular structure but also its composition. Apart from the lipid domain and keratin, water is also a major constituent of the SC and exists in the lipid matrix and corneocytes. Many transdermal permeation models are derived empirically by fitting experimental data and few are mechanistic. Published skin permeability models also considered the lipid matrix as the main pathway and regarded the corneocytes as impediments. These models under-predict

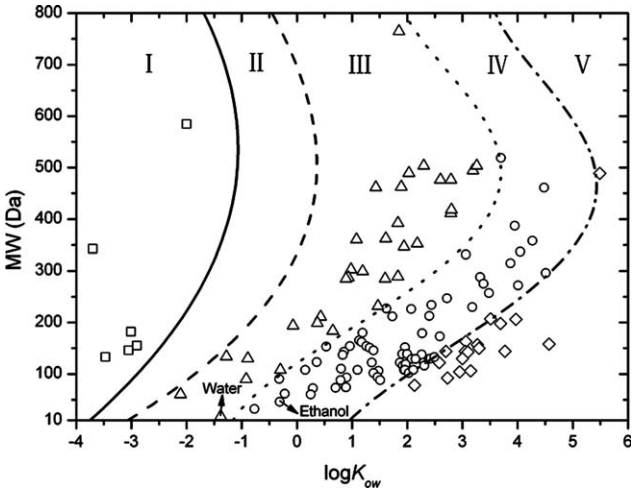

Figure 4. Mapping of the effect of tortuous lipid pathway and transcellular pathway on skin permeability in log $K_{ow} - M_W$ space.

I: $CP_I < 5\%$, $CP_T > 95\%$; II: $5\% \leq CP_I \leq 25\%$, $75\% \leq CP_T \leq 95\%$; III: $25\% \leq CP_I \leq 75\%$, $25\% \leq CP_T \leq 75\%$; IV: $75\% \leq CP_I \leq 95\%$, $5\% \leq CP_T \leq 25\%$; V: $95\% < CP_I$, $CP_T < 5\%$.

transdermal permeation of hydrophilic solutes by 2–3 orders of magnitude. In this study, we apply a recently developed model to predict the transdermal permeability of both hydrophilic and hydrophobic compounds. Solute permeation through the SC is modeled as mass transfer in the complex media of ''bricks-and-mortar,'' representing the discrete corneocytes and the continuous lipids matrix. Equations have been proposed for the complex partition and diffusion properties of solutes in both lipid matrix and corneocytes, allowing for closed-form prediction of skin permeability from the fundamental physical-chemical properties of solutes. It is shown that when compared with many previously reported models, the current model gives much improved prediction of skin permeability with $R^2 = 0.74$ and MSE $= 0.29$. In particular, the current model improved the prediction of highly hydrophilic solutes significantly by 2–3 orders of magnitude. The contribution of each pathway to overall skin permeability has also been analyzed. The results showed that the transcellular pathway is not only important for skin permeability of highly hydrophilic solutes, but for that of moderately hydrophobic solutes. The complex interaction of the two pathways can be mapped into five regions in the log $K_{ow} - M_W$ space with the contributions of the continuous lipid pathway accounting for 0–5%, 5–25%, 25–75%, 75–95%, and 95–100%, respectively. Another advantage of the current model is that it allows the analysis of skin hydration and miniaturization on transdermal permeation. In the following article, we will further discuss the application of the current model for closed-form prediction of dermatopharmacokinetic absorption and bioavailability of topically administered solutes in vivo.

Acknowledgments

This research is jointly supported by Unilever R&D Colworth and China Agricultural University (Contract No. 2008005).

Literature Cited

1. Johnson ME, Blankschtein D, Langer R. Evaluation of solute permeation through the stratum corneum: lateral bilayer diffusion as the primary transport mechanism. *J Pharm Sci*. 1997;86:1162–1172.
2. Mitragotri S. Modeling skin permeability to hydrophilic and hydrophobic solutes based on four permeation pathways. *J Control Rel*. 2003;86:69–92.
3. Pudney PDA, Mélot M, Caspers PJ, Van Der Pol A, Puppels GJ. An in vivo confocal raman study of the delivery of trans-retinol to the skin. *Appl Spectrosc*. 2007;61:804–811.
4. Stinchcomb AL, Pirot F, Touraille GD, Bunge AL, Guy RH. Chemical uptake into human stratum corneum in vivo from volatile and non-volatile solvents. *Pharm Res*. 1999;16:1288–1293.
5. Langer R, Peppas NA. Advances in biomaterials, drug delivery, and bionanotechnology. *AIChE J*. 2003;49:2990–3006.
6. Abraham MH, Chadha HS, Mitchell RC. The factors that influence skin penetration of solutes. *J Pharm Pharmacol*. 1995;47:8–16.
7. Abraham MH, Martins F, Mitchell RC. Algorithms for skin permeability using hydrogen bond descriptors: the problem of steroids. *J Pharm Pharmacol*. 1997;49:858–865.
8. Barratt MD. Quantitative structure activity relationships for skin corrosivity of organic acids, bases and phenols. *Toxicol in Vitro*. 1995;75:169–176.
9. Lien EJ, Gao H. Qsar analysis of skin permeability of various drugs in man as compared to in-vivo and in-vitro studies in rodents. *Pharm Res*. 1995;12:583–587.
10. Mitragotri S. A theoretical analysis of permeation of small hydrophobic solutes across the stratum corneum based on scaled particle theory. *J Pharm Sci*. 2002;91:744–752.
11. Potts RO, Guy RH. Predicting skin permeability. *Pharm Res*. 1992;9:663–669.
12. Potts RO, Guy RH. A predictive algorithm for skin permeability: the effects of molecular size and hydrogen bond activity. *Pharm Res*. 1995;12:1628–1633.
13. Wilschut A, Tenberge WF, Robinson PJ, T.E. M. Estimating skin permeation—the validation of 5 mathematical skin permeation models. *Chemosphere*. 1995;30:1275–1296.
14. Moss GP, Dearden JC, Patel H, Cronin MTD. Quantitative structure-permeability relationships (qsprs) for percutaneous absorption. *Toxicol In Vitro*. 2002;16:299–317.
15. Degim IT. New tools and approaches for predicting skin permeability. *Drug Discov Today*. 2006;11:517–523.
16. Cronin MTD, Dearden JC, Moss GP, Murray-Dickson G. Investigation of the mechanism of flux across human skin in vitro by quantitative structure-permeability relationships. *Eur J Pharm Sci*. 1999;7:325–330.
17. Abraham MH, Martins F. Human skin permeation and partition: general linear free-energy relationship analyses. *J Pharm Sci*. 2004;93:1508–1523.
18. Lian GP, Chen LJ, Han LJ. An evaluation of mathematical models for predicting skin permeability. *J Pharm Sci*. 2008;97:584–598.
19. Watkinson AC, Bunge AL, Hadgraft J, Naik A. Computer simulation of penetrant concentration-depth profiles in the stratum corneum. *Int J Pharm*. 1992;87:175–182.
20. Manitz R, Lucht W, Strehmel K, Weiner R, Neubert R. On mathematical modeling of dermal and transdermal drug delivery. *J Pharm Sci*. 1998;87:873–879.
21. Herkenne C, Naik A, Kalia YN, Hadgraft J, Guy RH. Dermatopharmacokinetic prediction of topical drug bioavailability in vivo. *J Invest Dermatol*. 2007;127:887–894.
22. Michaels AS, Chandrasekaran SK, Shaw JE. Drug permeation through human skin-theory and in-vitro experimental measurement. *AIChE J*. 1975;21:985–996.
23. Albery WJ, Hadgraft J. Percutaneous absorption in-vivo experiments. *J Pharm Pharmacol*. 1979;31:140–147.
24. Heisig M, Lieckfeldt R, Wittum G, Mazurkevich G, Lee G. Non steady-state descriptions of drug permeation through stratum corneum. 1. The biphasic brick-and-mortar model. *Pharm Res*. 1996;13:421–426.
25. Tojo K. Random brick model for drug transport across stratum corneum. *J Pharm Sci*. 1987;76:889–891.
26. Wang TF, Kasting GB, Nitsche JM. A multiphase microscopic diffusion model for stratum corneum permeability. I. Formulation, solution, and illustrative results for representative compounds. *J Pharm Sci*. 2006;95:620–648.
27. Wang TF, Kasting GB, Nitsche JM. A multiphase microscopic diffusion model for stratum corneum permeability. II. Estimation of physicochemical parameters and application to a large permeability database. *J Pharm Sci*. 2007;96:3024–3051.
28. Chen LJ, Lian GP, Han LJ. Use of ''bricks and mortar'' model to predict transdermal permeation: model development and initial validation. *Ind Eng Chem Res*. 2008;47:6465–6472.
29. Caspers PJ, Lucassen GW, Bruining HA, Puppels GJ. Automated depth-scanning confocal Raman microspectrometer for rapid in vivo determination of water concentration profiles in human skin. *J Raman Spectrosc*. 2000;31:813–818.
30. Anderson BD, Raykar PV. Solute structure-permeability relationships in human stratum corneum. *J Invest Dermatol*. 1989;93:280–286.
31. Mitragotri S, Johnson ME, Blankschtein D, Langer R. An analysis of the size selectivity of solute partitioning, diffusion, and permeation across lipid bilayers. *Biophys J*. 1999;77:1268–1283.
32. Kasting GB, Barai ND, Wang TF, Nitsche JM. Mobility of water in human stratum corneum. *J Pharm Sci*. 2003;92:2326–2340.
33. Johnson EM, Berk DA, Jain RK, Deen WM. Hindered diffusion in agarose gels: test of effective medium model. *Biophys J*. 1996;70:1017–1026.
34. Einstein A. Uber die von der molekular-kineticshen theorie der warme geforderte bewegung von in ruhenden flussigkeiten suspendierten teilchen. *Ann Physik*. 1905;17:549–560.

35. Jackson GW, James DG. The permeability of fibrous porous media. *Can J Chem Eng*. 1986;64:362–374.
36. Patel H, Ten BW, Cronin MTD. Quantitative structure-activity relationships (QSARs) for the prediction of skin permeation of exogenous chemicals. *Chemosphere*. 2002;48:603–613.
37. Sznitowska M, Berner B. *Polar pathway for percutaneous absorption*. In: Surber C, Elsner P, Bircher AJ, editors. *Exogenous Dermatology*. Basel: Karger; 1995:164–170.
38. Flynn GL. *Physiochemical determinants of skin absorption*. In Gerity TR, Henry CJ, editors. *Principles of Route-to-Route Extrapolation for Risk Assessment*, Amsterdam: Elsevier; 1990:93–127.
39. EDETOX. EDETOX database. Available at: http://edetox.ncl.ac.uk/. Accessed June 10, 2008.
40. Talreja PS, Kasting GB, Kleene NK, Pickens WL, Wang TF. Visualization of the lipid barrier and measurement of lipid pathlength in human stratum corneum. *AAPS PharmSci*. 2001;3:1–9.
41. Bouwstra JA, de Graaff A, Gooris GS, Nijsse J, Wiechers JW, van Aelst AC. Water distribution and related morphology in human stratum corneum at different hydration levels. *J Invest Dermatol*. 2003;120:750–758.
42. Warner RR, Myers MC, Taylor DA. Electron-probe analysis of human skin: determination of the water concentration profile. *J Invest Dermatol*. 1988;90:218–224.

Manuscript received Feb. 11, 2009, and revision received July 6, 2009.